S. Rastegari, E. Salahinejad, *Surface modification of Ti-6Al-4V alloy for osseointegration by alkaline treatment and chitosan-matrix glass-reinforced nanocomposite coating*, Carbohydrate polymers, 205 (2019) 302-311.
https://doi.org/10.1016/j.carbpol.2018.10.082

Surface modification of Ti-6Al-4V alloy for osseointegration by alkaline treatment and chitosan-matrix glass-reinforced nanocomposite coating

S. Rastegari, E. Salahinejad*

Faculty of Materials Science and Engineering, K. N. Toosi University of Technology, Tehran, Iran

Abstract

Individual and combined treatments of alkaline (NaOH) and chitosan/bioactive glass (SiO_2-CaO-MgO) nanocomposite coating were applied on Ti-6Al-4V alloy surfaces with the objective of investigating and improving i) wettability, ii) apatite-formation ability, iii) corrosion resistance, and iv) biocompatibility. Individual applications of each surface treatment were found to enhance hydrophilicity, apatite-forming ability, corrosion resistance, and cytocompatibility (MG-63 cells). The most improved properties, except apatite-formation ability, were obtained using the combined treatment yielding a reduction of 64 and 93 % in sessile contact angle and corrosion rate, respectively, than the untreated substrate. These improvements originate from the desired roughness and apatite-formation ability of the alkaline treatment and the appropriate biocompatibility and corrosion protection of the nanocomposite coating. That is, the combined application of alkaline treatment and chitosan

---

* Corresponding Author: Email Address: <salahinejad@kntu.ac.ir>

nanocomposite coating is demonstrated as a promising surface-engineering strategy for hard-tissue replacement applications.

Keywords**:** Titanium alloys; Surface modification; Chitosan; Osseointegration

1. Introduction

Medical-grade Ti-based alloys are currently used to augment or replace the structural components of the human body, due to their reasonable mechanical properties, corrosion resistance, and biocompatibility. However, there are clinical challenges still for Ti-based implants in terms of a direct bone-implant connection and long-term stabilization (Geetha, Singh, Asokamani, & Gogia, 2009; Khan, Williams, & Williams, 1999; Oshida, 2010). On the one hand, Ti-based implants passively integrate with the surrounding bone due to their bioinert nature, demanding a long period for osseointegration. On the other hand, Ti-based implants can suffer from electrochemical corrosion reactions, albeit at slow rates, accompanied by the release of ions toward the body, which can cause local irritation and inflammatory reactions (Ren, Dusad, Zhang, & Wang, 2013; Singh & Dahotre, 2007). To address these drawbacks, surface engineering approaches have been developed in terms of the alteration of the roughness and/or compositions of the surface (Davies, Ajami, Moineddin, & Mendes, 2013; F. He, Yang, Wang, & Zhao, 2009; Le Guéhennec, Soueidan, Layrolle, & Amouriq, 2007; Liu, Chu, & Ding, 2004; Mendonça, Mendonça, Aragao, & Cooper, 2008; Ponsonnet et al., 2003).

As one of the typical solutions, when Ti and its alloys are treated in a well-defined NaOH solution, the resultant surfaces show the ability to host a bone-like apatite layer and thus to bond tightly with the bone (Conforto, Caillard, Mueller, & Müller, 2008; H.-M. Kim, MIYAJI, KOKUBO, & NAKAMURA, 1997; H. M. Kim, Miyaji, Kokubo, & Nakamura, 1996). Nevertheless, the alkaline (NaOH) treatment creates a porous sodium titanate layer which releases Na^+ and raises the local pH upon immersion in physiological environments, thereby deteriorating the activity of living cells (J. Li et al., 2014). Another route is the application of a composite coating consisting of a suitable ceramic stimulating bone regeneration and a proper biopolymer exempting the need for an elevated-temperature densification process of the coating. Overall, this arrangement can mimic the composite structure of the natural bone. In this regard, SiO_2–CaO–MgO bioactive glasses are suitable candidates for the ceramic species since they present excellent biocompatibility, osteoinductivity, osteoconductivity, and apatite-formation ability at a desired speed (Diba, Goudouri, Tapia, & Boccaccini, 2014; Diba, Tapia, Boccaccini, & Strobel, 2012). Also, chitosan is a promising biopolymer for bone regeneration purposes, due to its biocompatibility, degradability and anti-bacterial properties (Muzzarelli, 2011). It has been also shown that chitosan-based composites encourage cell attachment, proliferation and differentiation as a result of a similarity between the chitosan and extra-cellular matrix structures (Karimi, Salahinejad, Sharifi, Nourian, & Tayebi, 2018; Zhao & Chang, 2004).

In this research, for the first time, a medical-grade Ti-based alloy (Ti-6Al-4V) was subjected to both the aforementioned surface treatments, i.e. alkaline treatment and chitosan/glass (SiO_2-CaO-MgO) nanocomposite coating. The hypothesis is that by employing the combined arrangement of the treatments, the surface benefits from the characteristics of both alkaline treating (desired roughness and apatite-formation ability) and nanocomposite coating (suitable biocompatibility and ion release alteration).

2. Materials and methods

2.1. Materials

The materials used in this study include: medical-grade Ti-6Al-4V alloy, NaOH (Merck, Germany, >97%), $SiCl_4$ (Merck, Germany, >99%), $MgCl_2$ (Merck, Germany, >98%), $CaCl_2$ (Merck, Germany, >98%), ethanol (Merck, Germany, >99.9%), NH_4OH Solution (Merck, Germany, 25%), chitosan (Sigma Aldrich, deacetylation degree: 84.2%, molecular weight: 140469.4 g/mol (Garcia et al., 2018)), and acetic acid (Mojallali, Iran, >99.9%).

2.2. Methods

Four types of surface treatments were applied on medical-grade Ti-6Al-4V alloy, as follows. As the common step of all the treatments, the substrates were polished and then cleaned with ethanol, acetone and distilled water (named as Ti). The surface-prepared substrates were immersed in a NaOH solution (5 M) at 60 °C for 24 h, followed by washing with distilled water and drying at 60 °C for 24 h (named as A-Ti). $2SiO_2$-CaO-MgO glass powders were synthesized by a coprecipitation method similar to Ref. (Baghjeghaz & Salahinejad, 2017), followed by calcination at 500 °C for 2 h, giving an amorphous structure (Esmati, Khodaei, Salahinejad, & Sharifi, 2018; Namvar et al., 2017). Chitosan (1.00 g) was dissolved in 1000 mL of 2.0% acetic acid aqueous solution. Calcined SiO_2-CaO-MgO powder (1.00 g) was subsequently added to the chitosan solution. The mixture was stirred using a magnetic stirrer for three hours and sonicated for 1 hour (Qsonica, Q125, Power Rating = 125 Watts, Frequency = 20 kHz) to provide a uniform dispersion of the powder in the chitosan solution. The obtained chitosan/glass sol was three times deposited through a dip coating method on both the above surface-polished and alkali-treated specimens, named as C-Ti and C-A-Ti, where each layer was dried at 40 °C for 24 h before applying the next layer. Eventually, to decease the effect of acetic acid on the surfaces, the coated samples were rinsed with a 0.1 M NaOH solution and then distilled water.

The surface morphology of the different samples was observed by field-emission scanning electron microscopy (FESEM, MIRA3TESCAN-XMU, accelerating voltage = 15 kV) after conventional gold spattering. The wettability of the prepared surfaces with respect to the simulated body fluid (SBF), as a characteristic affecting biocompatibility, was determined by sessile contact angle measurements in air, with a repetition of three times.

For the apatite-formation ability assessment of the surfaces, the prepared samples were soaked in the SBF at 37 °C for 7 days without refreshing the medium. Then, the immersed surfaces were observed by FESEM equipped with energy-dispersive X-ray spectroscopy (EDS). Also, the concentration of ions in the SBF before and after contact with the samples was measured by inductively coupled plasma spectroscopy (ICP-OES, OES-730, Varian).

The corrosion behavior of the samples was investigated by a potentiostat/galvanostat (Vertex, Ivium Technologies) using a platinum wire cathode and Ag/AgCl reference electrode. To do so, the samples were first kept in the SBF for 2 h in order to obtain a steady-state condition. Electrochemical impedance spectroscopy (EIS) was conducted with an potential amplitude of 10 mV vs. the open circuit potential from 10 kHz to 0.01 Hz. Afterwards, potentiodynamic polarization curves were obtained at a scan rate of 0.1 mV/s, where the related electrochemical data were determined by the Tafel extrapolation of the anodic and cathodic branches. The accuracy of the voltage and current measurements was 0.01%.

For biocompatibility assessments, osteoblast-like MG-63 cells (Pastor Institute, Iran) were cultured in the Dulbecco's modified Eagle's medium, supplemented with fetal bovine serum (Gibco) and antibiotic (penicillin/streptomycin, Gibco) solution under a humidified atmosphere of 5 % CO_2 at 37 °C. Prior to testing, the samples were soaked in a 70% ethanol solution for 2 hours, rinsed with the phosphate-buffered saline solution, and then UVsterilized for 20 min. A concentration of 2.00×10^4 cell/well was used for the culture durations of 24 and 48 hours. To evaluate cell viability, the optical density (OD) of viable cells was measured by the MTT assay. A filtered MTT solution (5 mg/ml, Sigma Aldrich) was added to each well, and the cells were incubated at 37 C for 4 h. After the complete removal of the culture medium, dimethyl sulfoxide (1:1, v/v, Amresco, Solon, USA) was added to each well to dissolve colored products into the solution. The optical density of the purple product in the solution was measured using a spectrometer UV (Stat Fax- 2100) set at 570 nm. Three replicates were conducted for each sample, and the analysis of variance was performed with a significance level of $p < 0.05$. Also, the morphology of the cultured MG-63 cells was observed by a SEM.

3. Results and discussion

The FESEM micrographs of the various surfaces are presented in Fig. 1 in two magnifications. As can be seen in Figs. 1(c) and 1(d), a relatively non-agglomerated and homogeneous distribution of the glassy nanoparticles having a mean size of 50 nm in the crack-free chitosan matrix was obtained for the composite coating surface (C-Ti). Figs. 1(e) and 1(f) also show the surface morphology of the alkaline-treated substrate (A-Ti), which is characterized as a crack-free, uniform and feather-like layer of mostly sodium titanate (Kokubo & Yamaguchi, 2010; Yamaguchi, Takadama, Matsushita, Nakamura, & Kokubo, 2009). Typically, interconnected blades of 70 nm in thickness have made feather-like porous networks with a mean hollow size of 200 nm. The surface subjected to both the alkaline treatment and composite coating (C-A-Ti) exhibits a uniform distribution of the nanoparticles on the feather-like alkaline-treated plates (Figs. 1(g) and 1(h)). In conclusion, all the micrographs display desirable features for the prepared surfaces.

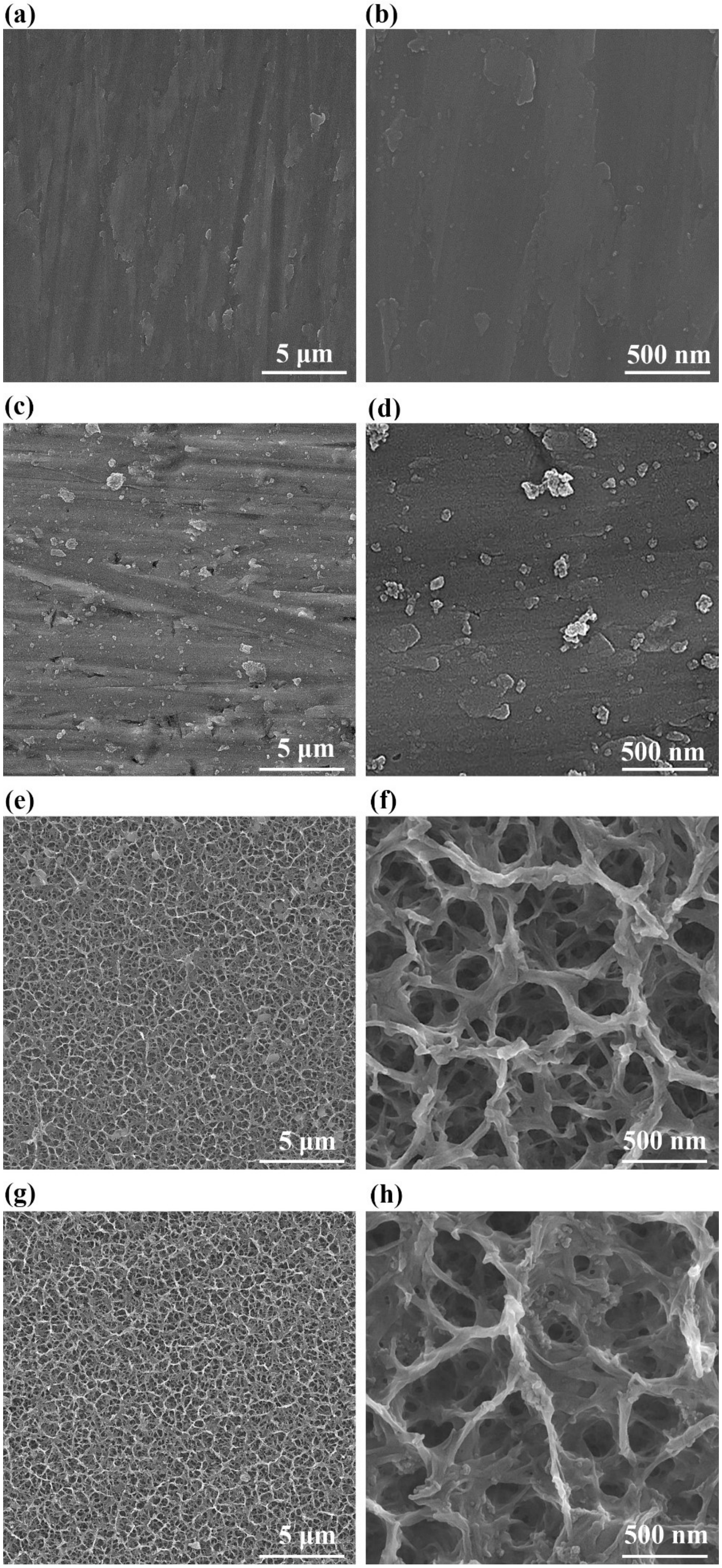
(a)
5 µm
(b)
500 nm
(c)
5 µm
(d)
500 nm
(e)
5 µm
(f)
500 nm
(g)
5 µm
(h)
500 nm

Fig. 1. FESEM micrographs of the sample surfaces: Ti (a, b), C-Ti (c, d), A-Ti (e, f), and C-A-Ti (g, h).

Figs. 2(a) to 2(d) represent the side-view macrographs of the SBF droplets on the processed surfaces. The related mean sessile contact angles are also represented in Fig. 2(e), with the following hydrophilicity ranking: C-A-Ti > A-Ti > C-Ti > Ti. This suggests the positive effects of the alkaline treatment and chitosan/glass coating on the wettability of the titanium surface, where the highest improvement is obtained after the combined surface treatments. The polished Ti surface is immediately covered by a passive oxide layer upon exposure to air or corrosive environments. This layer considerably tends to attract water via OH^- groups, as called "hydration of titanium surface", thereby enhancing the surface energy and wettability (Kokubo & Yamaguchi, 2009). Chitosan also presents wettability in contact with water, because of interactions between its positive-charged amine groups and OH^- ions (Lin & Chen, 2013). The inherent hydrophilicity of glasses and glass-ceramics also originates from the existence of hydroxyl groups on their surface, via establishing a hydrogen bonding with water molecules (Takeda, Yamamoto, Hayasaka, & Matsumoto, 1999). That is, the chitosan/glass coating in the C-Ti sample increases the wettability of the Ti substrate. However, the alkaline-treated surface (A-Ti) benefits from a higher wettability, due to both a higher surface roughness (Fig. 1) and an increased surface energy attributed to surface Ti-OH groups (Lu et al., 2008; Yamaguchi et al., 2009). Finally, the combined effect of the high roughness of the alkaline-treated surface (realized from the microscopic observations) and the high surface energy of the composite coating dictates the highest wettability for the C-A-Ti sample.

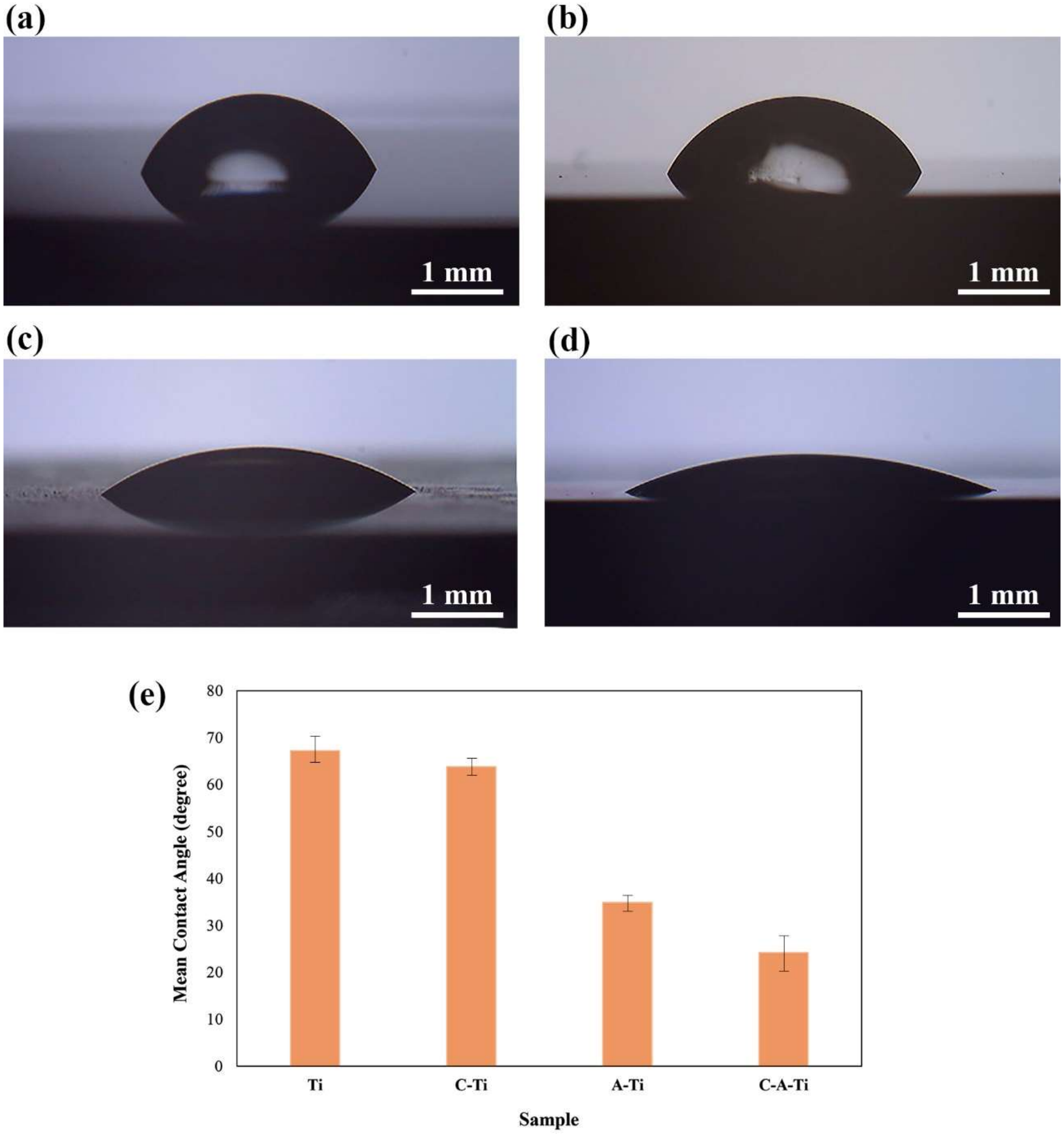

Fig. 2. Macrographs of the SBF droplets on the samples: Ti (a), C-Ti (b), A-Ti (c), and C-A-Ti (d) and related contact angles (e).

After immersion of the samples in the SBF for 7 days, the surfaces were examined by FESEM-EDS (Fig. 3). According to Figs. 3(a) and 3(b), limited regions of the Ti surface have been covered by thin precipitates of apatite. Indeed, upon immersion in the SBF, the passive layer of the Ti surface is subjected to hydration accompanied by surface Ti-OH groups. This

S. Rastegari, E. Salahinejad, *Surface modification of Ti-6Al-4V alloy for osseointegration by alkaline treatment and chitosan-matrix glass-reinforced nanocomposite coating*, Carbohydrate polymers, 205 (2019) 302-311.
https://doi.org/10.1016/j.carbpol.2018.10.082

surface negative charge leads to the alternate adsorption of calcium and phosphate ions from the SBF, forming an apatite layer (P. Li et al., 1994). Comparatively, on the C-Ti sample surface soaked in the SBF, a higher level of nanospherical apatite precipitation, albeit accumulated around the glass nanoparticles, is observed (Figs. 3(d) and 3(e)). This type of apatite precipitation is essentially achieved through the ion exchange of Ca^{2+} and Mg^{2+} of the ceramic with H_3O^+ of the SBF, the formation of surface silanol (Si-OH) and thereby the adsorption of Ca and PO_4^{3-} ions (Rahmani & Salahinejad, 2018; E Salahinejad & Baghjeghaz, 2017; Erfan Salahinejad & Vahedifard, 2017; Vahedifard & Salahinejad, 2017). However, the alkaline-treated (A-Ti) sample has been thoroughly covered with apatite with a flower-like morphology, based on Figs. 3(g) and 3(h). In this regard, Na^+ of the alkaline-treated surface is exchanged with H_3O^+ of the SBF, thereby forming Ti-OH groups on the Ti surface and encouraging the precipitation of an apatite layer (Yamaguchi et al., 2009). Figs. 3(j) and 3(k) demonstrate that the deposition of the composite coating on the alkaline-treated surface has reduced apatite-formation ability, in comparison to the A-Ti sample, where apatite accumulation around the nanoparticles is dominant. This is due to the lower apatite-formation ability of chitosan, compared to the MgO-SiO_2-CaO glass and sodium titanate. The presence of P in the EDS patterns of the immersed samples infers the precipitation of a calcium phosphate (apatite) phase as a result of contact between the samples and SBF, because all the surfaces were P-free before immersion. The comparison of the intensity of P in the EDS patterns, in good agreement with the FESEM micrographs, demonstrates that apatite-formation is improved *in vitro* in the order: Ti, C-Ti, C-A-Ti, and A-Ti.

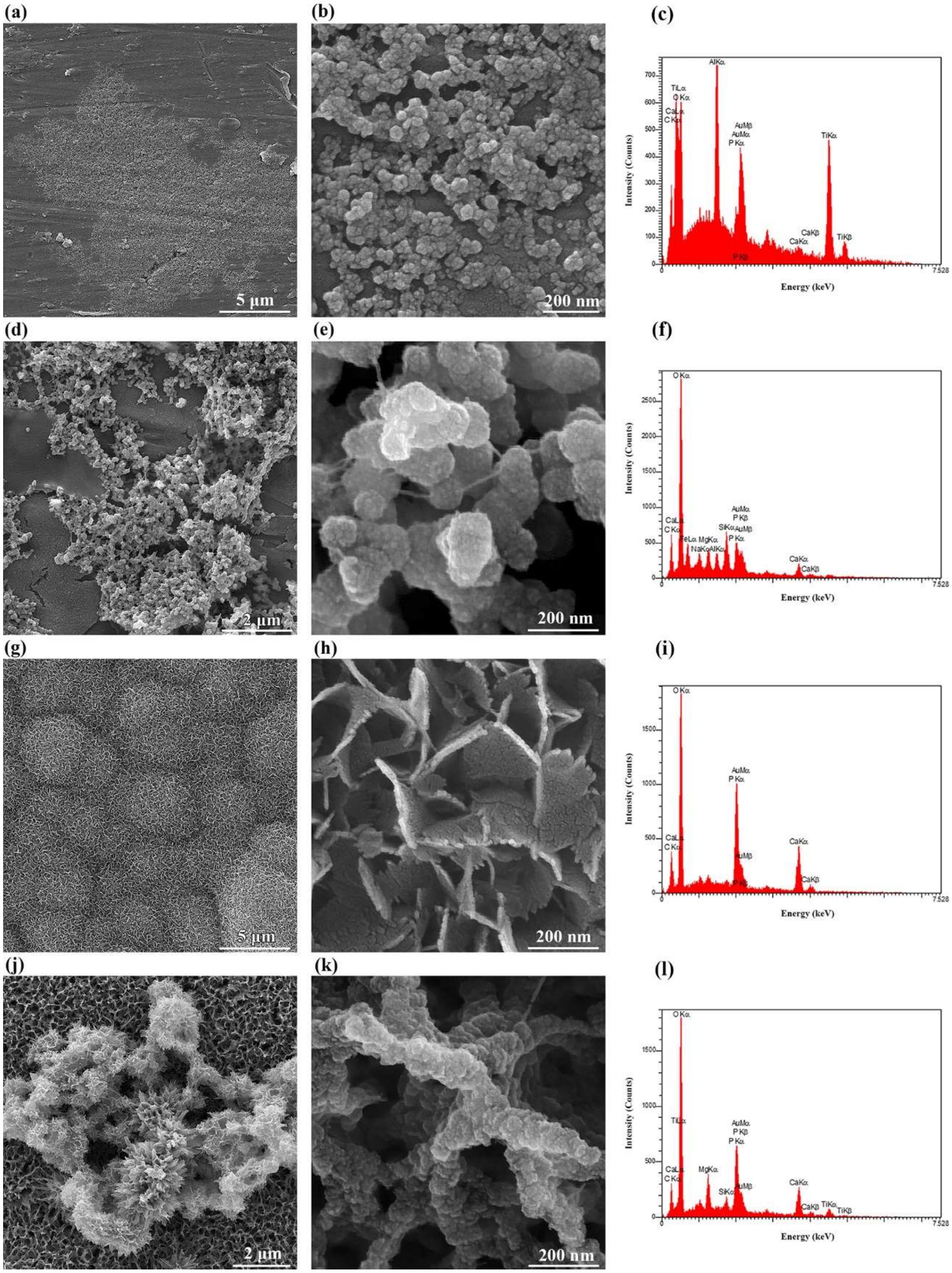

Fig. 3. FESEM micrographs (in two magnifications) and EDS spectra of the samples after immersion in the SBF: Ti (a, b, c), C-Ti (d, e, f), A-Ti (g, h, i), and C-A-Ti (j, k, l).

The concentration of Ca^{2+}, P^{3+}, Si^{4+} and Mg^{2+} in the SBF in contact with the surface-modified samples was measured by ICP (Fig. 4). As can be seen, for both the composite-coated samples (C-Ti and C-A-Ti), the concentrations of Si and Mg ions increased after immersion, due to the degradation of the silicate glass nanoparticles. In contrast, the concentration of P and Ca ions shows a decline due to the apatite precipitation. These variations in the level of the ions suggest that an ion-exchange mechanism is responsible for apatite precipitation. Also, in contrast to Ca, since the samples were P-free, the reduction of the P concentration is indicative of the level of apatite deposition and can be regarded as a valid criterion to compare the apatite-forming ability. Thus, based on the ICP analysis, the apatite-forming ability varies as follows: A-Ti > C-A-Ti > C-Ti > Ti, which is in good agreement with the FESEM-EDS analyses.

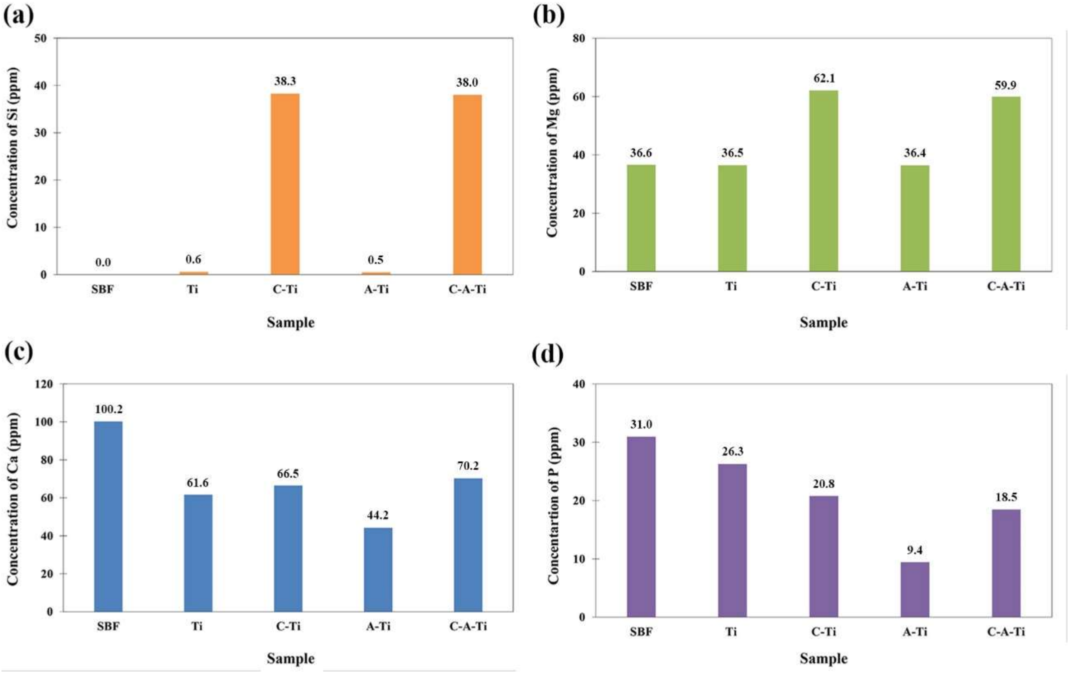

Fig. 4. ICP results on the SBFs in contact with the samples for Si (a), Mg (b), Ca (c), and P (d) ions (the estimated error is 0.1 ppm).

The EIS Nyquist and Bode plots of the samples in the SBF at 37 °C are depicted in Fig. 5. The surface-treated (C-Ti, A-Ti, and C-A-Ti) samples present an almost linear (or a semi-circle of high radii) Nyquist curve, whereas Ti exhibits a typical semi-circle curve. Comparatively, at any real part of impedance, the imaginary parts and thereby the corrosion resistance in the SBF increase in the following ranking: Ti < C-Ti < A-Ti < C-A-Ti. Essentially, titanium forms a passive oxide film on its surface once it is exposed to a corrosive environment. Although this passive layer is adhesive, the Nyquist curve illustrates a penetrable character for this film. Vanadium as one of the alloying elements of the Ti sample develops an unstable oxide which can be dissolved in the presence of Cl^- ions existing in the SBF, giving rise to the damage of the passive layer (Shukla & Balasubramaniam, 2006). The Nyquist curves of the C-Ti and A-Ti samples show higher corrosion resistances than Ti, owing to a more protective behavior of the related surface layers. However, the highest corrosion resistance belongs to the C-A-Ti sample since this sample benefits from both the surface treatments providing physical barriers against the SBF access.

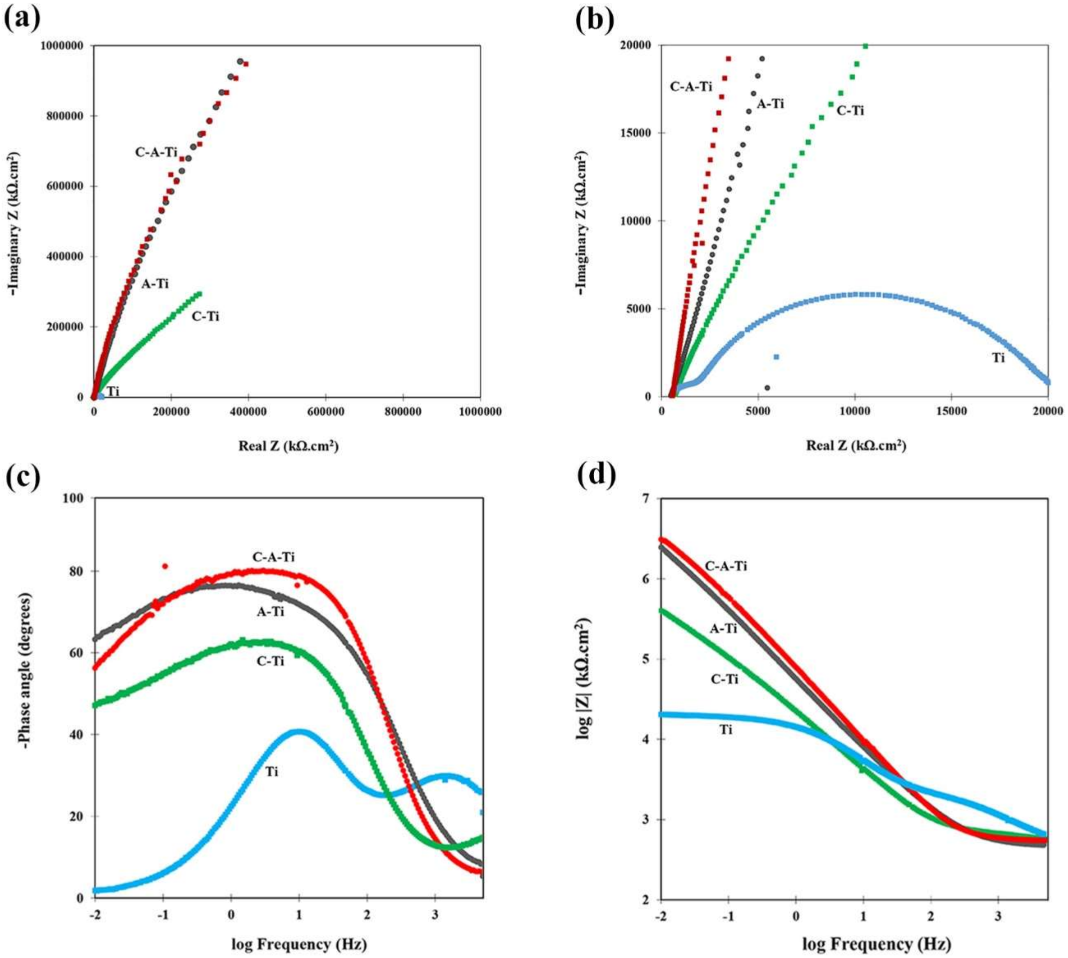

Fig. 5. EIS results in terms of: Nyquist (a), magnified Nyquist (b), Bode-phase angle (c), and Bode-impedance magnitude (d) plots.

According to Fig. 5(c), the Bode-phase angle curve of the Ti sample exhibits two peaks, i.e. a two time-constant behavior, which is attributed to two imperfect surface layers. The first time constant at low frequencies is related to the continuous passive layer of TiO_2 formed on the substrate, whereas the second time constant at higher frequencies is attributed to an outer non-continuous porous layer of apatite precipitated casually on the surfaces during exposure in the SBF (Alves et al., 2017; Fazel, Salimijazi, & Golozar, 2015). For the C-Ti, A-Ti and C-

A-Ti samples, the Bode-phase angle curve shows a maximum as a sign of a capacitor behavior, suggesting higher corrosion resistances in comparison to Ti. The Bode-impedance magnitude curve (Fig. 5(d)) at higher frequencies exhibits a plateau feature, which corresponds to that region of the Bode-phase plot with a tendency towards zero, demonstrating electrolyte polarization resistance (Alves et al., 2017). The figure also indicates that over the entire range of the applied frequency, the impedance magnitude and thereby corrosion resistance follow the ranking: C-A-Ti > A-Ti > C-Ti > Ti, which is compatible with the conclusion drawn from the Nyquist curve.

Fig. 6 indicates the potentiodynamic polarization curves of the samples in the SBF. Using the IviumSoft software, the corrosion current densities were determined from the extrapolation of the cathodic and anodic branches of the Tafel regions. Also, the related corrosion rates were calculated according to Equation 1 (Kewen Cai et al., 2016):

$$\mathrm{CR} = \frac{\mathrm{K}\ \mathrm{i}_{\mathrm{corr}}\ \mathrm{M}}{\mathrm{D\ V}} \tag{1}$$

where CR is the corrosion rate in mm/year, K is a constant (= 0.00327), i_{corr} is the corrosion current density ($\mu A/cm^2$), M is the molecular weight (gr/mole), V is the number of electrons transferred during the corrosion reactions, and D is the metal density (gr/cm^3). As tabulated in Table 1, based on the polarization tests, the corrosion resistance ranks as follows: C-A-Ti > A-Ti > C-Ti > Ti, which is in good agreement with the EIS results.

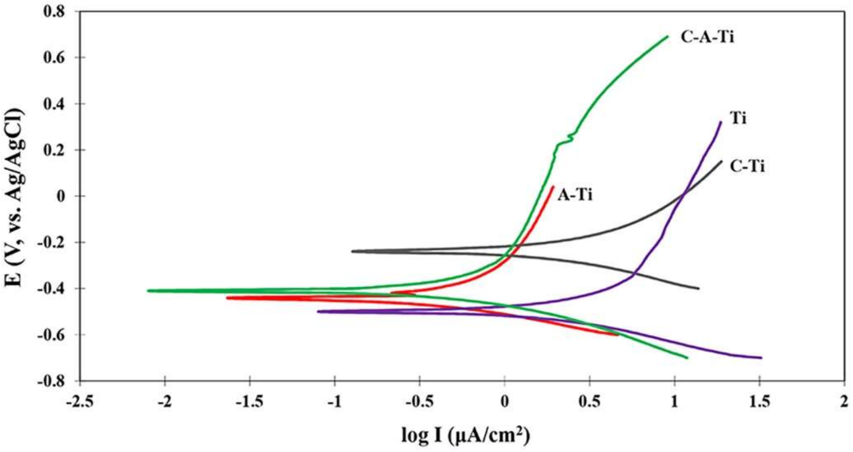

Fig. 6. Potentiodynamic polarization curves of the prepared samples.

Table 1. Electrochemical data extracted from the polarization curves (the estimated error is 0.01%).

Sample	i_{corr} **(µA/cm^2)**	***CR*** **(mm/year)**
Ti	20.6538	0.0113
C-Ti	6.4506	0.0070
A-Ti	1.4093	0.0013
C-A-Ti	1.2471	0.0008

Fig. 7 shows the results of the MTT assay on the MG-63 cell cultures, in terms of the optical density (OD) of viable cells. As can be seen, at 24 h, the OD values for all surface-treated samples are comparable to the biocompatible substrate with no significant differences, suggesting the cytocompatibility of the surfaces. The increase in the OD values from 24 h to 48 h also indicates cell proliferation on the surfaces, where the proliferation rate on the surfaces increases in the following order: C-Ti > C-A-Ti > A-Ti > Ti. Accordingly, after 48 h of culture, the OD and cell viability are altered into the following order: C-A-Ti > C-Ti > A-Ti > Ti.

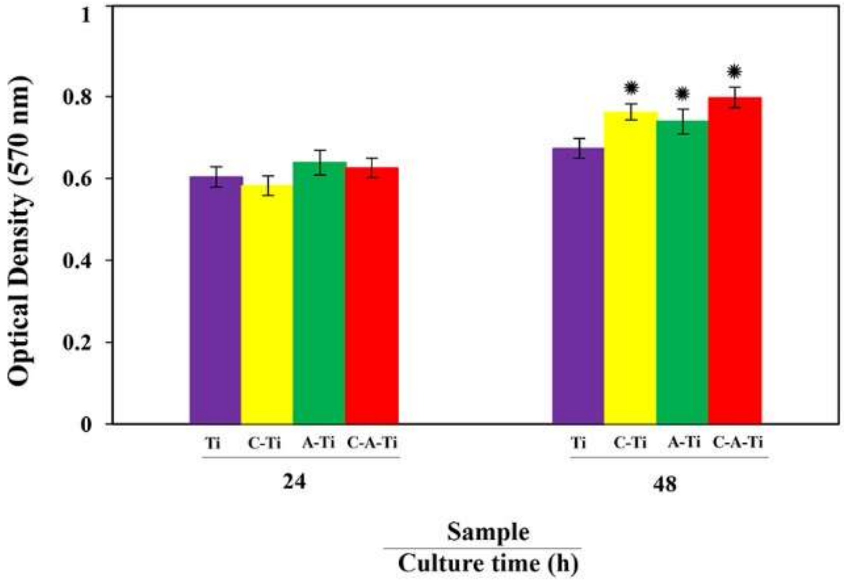

Fig. 7. MTT results in terms of OD. * represents $p < 0.05$ with respect to the untreated substrate (Ti).

It is well established that the Ti-6Al-4V alloy (the Ti sample regarded as the control in this study) is biocompatible due to the TiO_2 layer formed on its surface (Textor, Sittig, Frauchiger, Tosatti, & Brunette, 2001), which is more typical at the early stages of the cell culture (24 h). However, by progression of the cell culture, i.e. at 48 h of culture, the passive layer is likely to be penetrated by corrosion. This leads to the release of toxic vanadium cations from the Ti surface and limits the cell viability and proliferation. Regarding the C-Ti sample, on the one hand, the high biocompatibility levels of chitosan (Kaiyong Cai, Hu, Jandt, & Wang, 2008; Lin & Chen, 2013) and glass particles (Luz & Mano, 2012; Valerio, Pereira, Goes, & Leite, 2004) ensure the improved cell proliferation from 24 h to 48 h compared to the control. On the other hand, the corrosion protection improved by employing the composite coating, based on Figs. 5 and 6, limits the release of toxic vanadium cations, thereby enhancing the cell proliferation. The comparison of the results for these two samples suggests that the positive contribution of the composite coating is dominant at the higher culture periods (48 h). For the A-Ti sample, in comparison to the control, the nanometric topography (Fig. 1), high hydrophilicity (Fig. 2), and corrosion protection (Figs. 5 and 6) of the alkaline-treated layer guarantee the suitable interaction of cells, especially at the early stages of cell culture. However, by increasing the culture time, the release of Na^+ and its ionic exchange with H^+ of the medium cause a local increase in pH at the cell/implant interface, which is deteriorous for MG-63 cells (J. Li et al., 2014). This explains the lower proliferation rate of A-Ti compared to C-Ti. Eventually, the highest cell proliferation and cytocompatibility of the C-A-Ti sample are attributed to the following contributions:

i) The advantageous effect of the nanoscale rough topography provided by the alkaline treatment,

ii) The retarded release of sodium ions, as a result of the deposition of the composite coating on the alkaline-treated surface,

iii) The limited release of vanadium ions from the substrate by employing both the treatments, as inferred from Figs. 5 and 6,

iv) The advantageous release of Mg, Si and Ca ions and the beneficial contribution of the composite coating constitutes.

Fig. 8 demonstrates the SEM micrograph of the surfaces after 24 of the cell culture. As can be seen, the cell spreading on the Ti surface is relatively suitable due to its biocompatibility. The application of the composite coating has improved the cell spreading and adhesion on the C-Ti surface in comparison to Ti, whereas the cells are mostly round and are not entirely spread still. The improvement in the cell adhesion is continued for the A-Ti and then C-A-Ti samples. By increasing the cell culture period to 48 h (Fig. 9), for all of the samples, the cell adhesion and number (meaning cell proliferation) have been enhanced with developed cytoplasmic extensions.

Chitosan is a well-suited substrate for cell adhesion. The presence of the nanoparticles not only provides a bone-like biomimetic environment and activates cellular responses, but also increases the matrix stiffness and enhances adhesion to the implant surface (J. He et al., 2016). Collectively, the release of Mg, Si and Ca ions, higher roughness and hydrophilicity of the modified surfaces, and retardation of vanadium release originate from the application of the composite coating and alkaline treatment on titanium and have positive effects on cell responses. In summary, the comparison of the cell adhesion on the surfaces confirms the ranking realized by the MTT assay, where the highest biocompatibility is attributed to the C-A-Ti sample.

S. Rastegari, E. Salahinejad, *Surface modification of Ti-6Al-4V alloy for osseointegration by alkaline treatment and chitosan-matrix glass-reinforced nanocomposite coating*, Carbohydrate polymers, 205 (2019) 302-311.
https://doi.org/10.1016/j.carbpol.2018.10.082

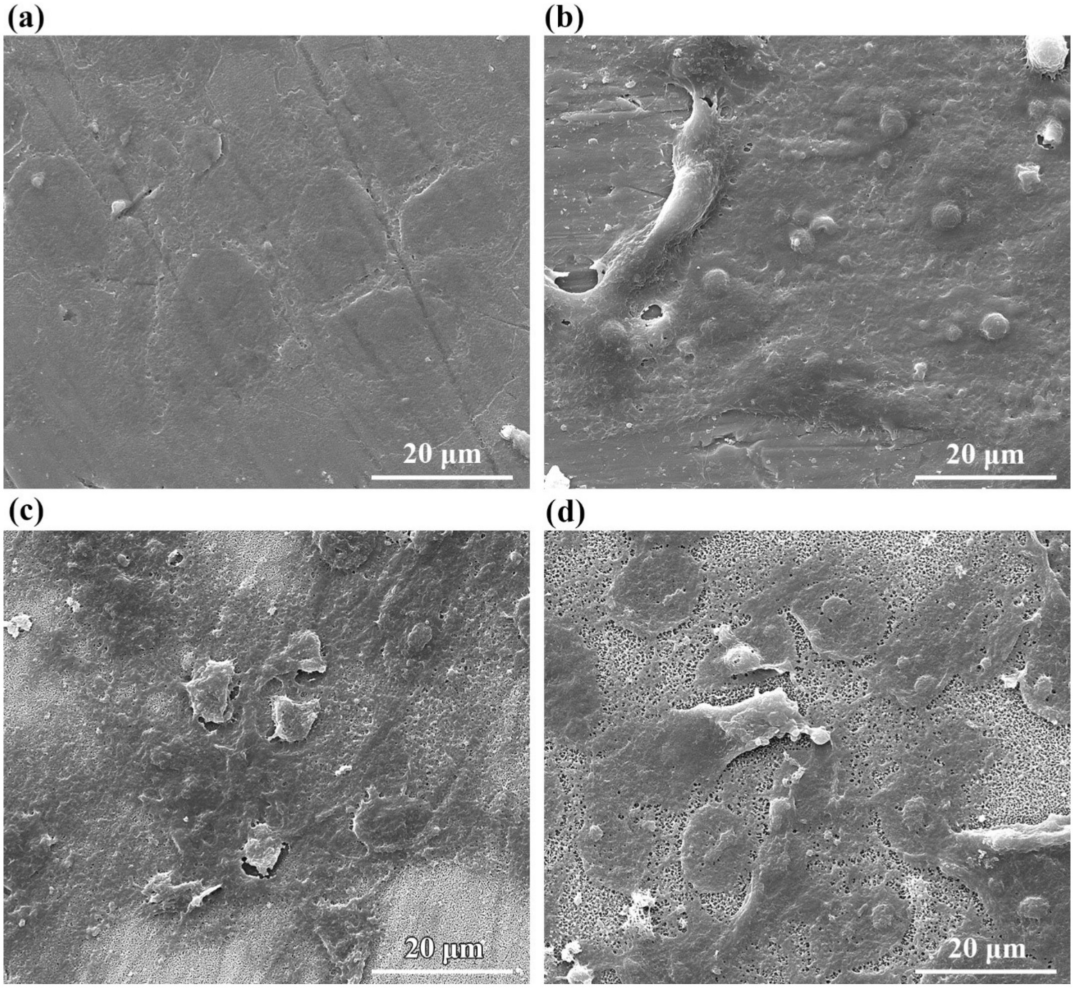

Fig. 8. SEM micrograph of the cell cultures for 24 h: Ti (a), C-Ti (b), A-Ti (c), and C-A-Ti (d).

This is the accepted manuscript (postprint) of the following article:
S. Rastegari, E. Salahinejad, *Surface modification of Ti-6Al-4V alloy for osseointegration by alkaline treatment and chitosan-matrix glass-reinforced nanocomposite coating*, Carbohydrate polymers, 205 (2019) 302-311.
https://doi.org/10.1016/j.carbpol.2018.10.082

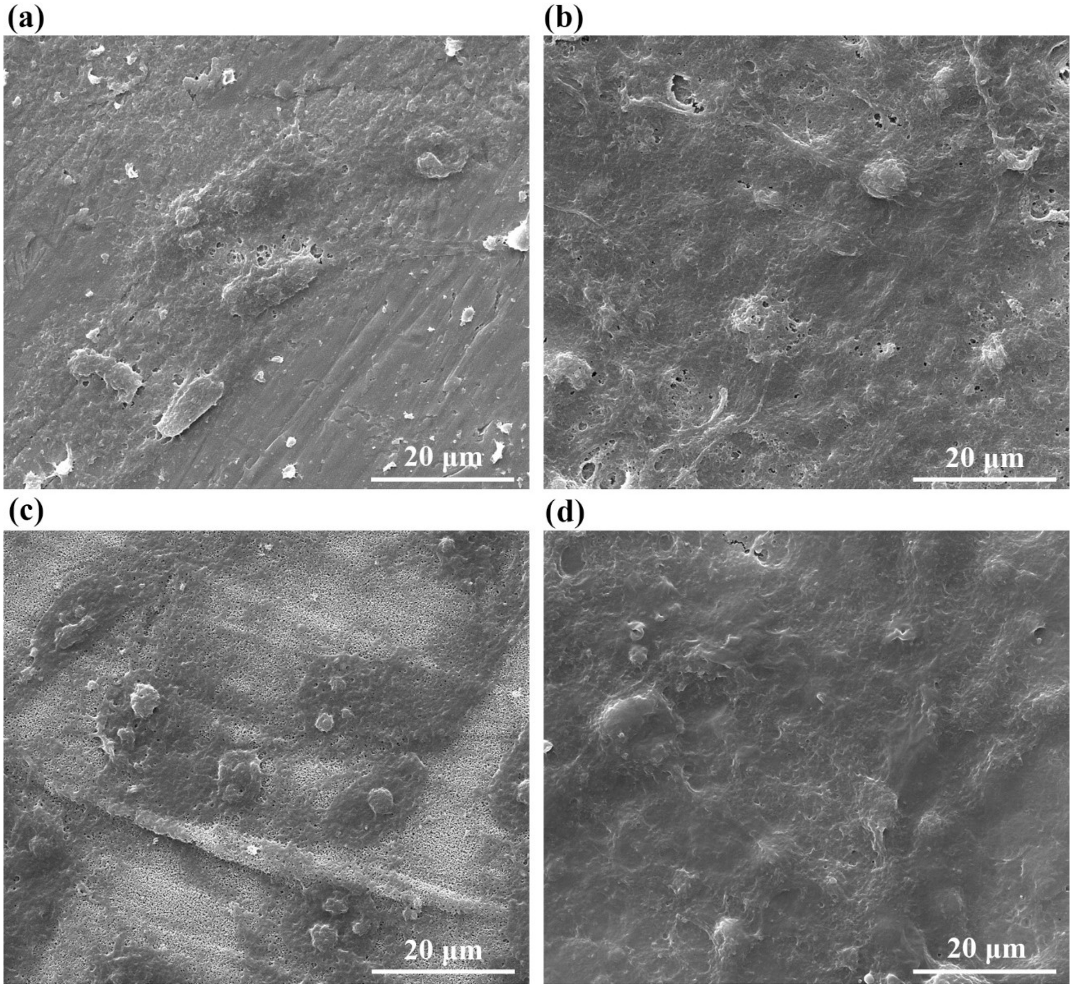

Fig. 9. SEM micrograph of the cell cultures for 48 h: Ti (a), C-Ti (b), A-Ti (c), and C-A-Ti (d).

4. Conclusions

Alkaline-treating and nanocomposite-coating were employed on Ti-6Al-4V alloy to improve the biological performance of. The parameters used for the surface treatments provided homogenous and crack-free morphologies. According to the results, the individual application of each surface treatment enhanced the surface wettability, apatite-formation ability, corrosion protection, cell viability, and cell adhesion of the substrate. The best performance (except apatite-formation ability which was comparatively realized to be highest for the alkaline-treated sample) was found for the sample subjected to both the treatment, i.e. alkaline-treating followed by composite-coating. Because this sample benefits from the advantageous effects of both alkaline treatment and the coating constitutes (chitosan and SiO_2-CaO-MgO glass). Albeit it is noticeable that the individual application of the alkaline treatment led to the highest apatite-formation ability.

References

Alves, A., Wenger, F., Ponthiaux, P., Celis, J.-P., Pinto, A., Rocha, L., & Fernandes, J. (2017). Corrosion mechanisms in titanium oxide-based films produced by anodic treatment. *Electrochimica Acta,* 234, 16-27.

Baghjeghaz, M. J., & Salahinejad, E. (2017). Enhanced sinterability and in vitro bioactivity of diopside through fluoride doping. *Ceramics International,* 43(5), 4680-4686.

Cai, K., Hu, Y., Jandt, K. D., & Wang, Y. (2008). Surface modification of titanium thin film with chitosan via electrostatic self-assembly technique and its influence on osteoblast growth behavior. *Journal of materials science: Materials in medicine,* 19(2), 499.

Cai, K., Zuo, S., Luo, S., Yao, C., Liu, W., Ma, J., . . . Li, Z. (2016). Preparation of polyaniline/graphene composites with excellent anti-corrosion properties and their application in waterborne polyurethane anticorrosive coatings. *RSC Advances,* 6(98), 95965-95972.

Conforto, E., Caillard, D., Mueller, L., & Müller, F. (2008). The structure of titanate nanobelts used as seeds for the nucleation of hydroxyapatite at the surface of titanium implants. *Acta biomaterialia,* 4(6), 1934-1943.

Davies, J. E., Ajami, E., Moineddin, R., & Mendes, V. C. (2013). The roles of different scale ranges of surface implant topography on the stability of the bone/implant interface. *Biomaterials,* 34(14), 3535-3546.

Diba, M., Goudouri, O.-M., Tapia, F., & Boccaccini, A. R. (2014). Magnesium-containing bioactive polycrystalline silicate-based ceramics and glass-ceramics for biomedical applications. *Current opinion in solid state and materials science,* 18(3), 147-167.

S. Rastegari, E. Salahinejad, *Surface modification of Ti-6Al-4V alloy for osseointegration by alkaline treatment and chitosan-matrix glass-reinforced nanocomposite coating*, Carbohydrate polymers, 205 (2019) 302-311.
https://doi.org/10.1016/j.carbpol.2018.10.082

Diba, M., Tapia, F., Boccaccini, A. R., & Strobel, L. A. (2012). Magnesium-containing bioactive glasses for biomedical applications. *International Journal of Applied Glass Science,* 3(3), 221-253.

Esmati, N., Khodaei, T., Salahinejad, E., & Sharifi, E. (2018). Fluoride doping into SiO2-MgO-CaO bioactive glass nanoparticles: bioactivity, biodegradation and biocompatibility assessments. *Ceramics International*.

Fazel, M., Salimijazi, H., & Golozar, M. (2015). A comparison of corrosion, tribocorrosion and electrochemical impedance properties of pure Ti and Ti6Al4V alloy treated by micro-arc oxidation process. *Applied Surface Science,* 324, 751-756.

Garcia, L. G. S., de Melo Guedes, G. M., da Silva, M. L. Q., Castelo-Branco, D. S. C. M., Sidrim, J. J. C., de Aguiar Cordeiro, R., . . . Brilhante, R. S. N. (2018). Effect of the molecular weight of chitosan on its antifungal activity against Candida spp. in planktonic cells and biofilm. *Carbohydrate Polymers*.

Geetha, M., Singh, A., Asokamani, R., & Gogia, A. (2009). Ti based biomaterials, the ultimate choice for orthopaedic implants–a review. *Progress in Materials Science,* 54(3), 397-425.

He, F., Yang, G., Wang, X., & Zhao, S. (2009). Bone responses to rough titanium implants coated with biomimetic Ca-P in rabbit tibia. *Journal of Biomedical Materials Research Part B: Applied Biomaterials,* 90(2), 857-863.

He, J., Meng, G., Yao, R., Jiang, B., Wu, Y., & Wu, F. (2016). The essential role of inorganic substrate in the migration and osteoblastic differentiation of mesenchymal stem cells. *Journal of the mechanical behavior of biomedical materials,* 59, 353-365.

Karimi, S., Salahinejad, E., Sharifi, E., Nourian, A., & Tayebi, L. (2018). Bioperformance of chitosan/fluoride-doped diopside nanocomposite coatings deposited on medical stainless steel. *Carbohydrate Polymers*.

Khan, M., Williams, R. L., & Williams, D. F. (1999). The corrosion behaviour of Ti–6Al–4V, Ti–6Al–7Nb and Ti–13Nb–13Zr in protein solutions. *Biomaterials,* 20(7), 631-637.

Kim, H.-M., MIYAJI, F., KOKUBO, T., & NAKAMURA, T. (1997). Apatite-forming ability of alkali-treated Ti metal in body environment. *Journal of the ceramic Society of Japan,* 105(1218), 111-116.

Kim, H. M., Miyaji, F., Kokubo, T., & Nakamura, T. (1996). Preparation of bioactive Ti and its alloys via simple chemical surface treatment. *Journal of Biomedical Materials Research Part A,* 32(3), 409-417.

Kokubo, T., & Yamaguchi, S. (2009). Novel bioactive titanate layers formed on Ti metal and its alloys by chemical treatments. *Materials,* 3(1), 48-63.

S. Rastegari, E. Salahinejad, *Surface modification of Ti-6Al-4V alloy for osseointegration by alkaline treatment and chitosan-matrix glass-reinforced nanocomposite coating*, Carbohydrate polymers, 205 (2019) 302-311. https://doi.org/10.1016/j.carbpol.2018.10.082

Kokubo, T., & Yamaguchi, S. (2010). Bioactive Ti metal and its alloys prepared by chemical treatments: state-of-the-art and future trends. *Advanced Engineering Materials,* 12(11).

Le Guéhennec, L., Soueidan, A., Layrolle, P., & Amouriq, Y. (2007). Surface treatments of titanium dental implants for rapid osseointegration. *Dental materials,* 23(7), 844-854.

Li, J., Wang, G., Wang, D., Wu, Q., Jiang, X., & Liu, X. (2014). Alkali-treated titanium selectively regulating biological behaviors of bacteria, cancer cells and mesenchymal stem cells. *Journal of colloid and interface science,* 436, 160-170.

Li, P., Ohtsuki, C., Kokubo, T., Nakanishi, K., Soga, N., & de Groot, K. (1994). The role of hydrated silica, titania, and alumina in inducing apatite on implants. *Journal of biomedical materials research Part A,* 28(1), 7-15.

Lin, H.-Y., & Chen, J.-H. (2013). Osteoblast differentiation and phenotype expressions on chitosan-coated Ti-6Al-4V. *Carbohydrate polymers,* 97(2), 618-626.

Liu, X., Chu, P. K., & Ding, C. (2004). Surface modification of titanium, titanium alloys, and related materials for biomedical applications. *Materials Science and Engineering: R: Reports,* 47(3), 49-121.

Lu, X., Wang, Y., Yang, X., Zhang, Q., Zhao, Z., Weng, L. T., & Leng, Y. (2008). Spectroscopic analysis of titanium surface functional groups under various surface modification and their behaviors in vitro and in vivo. *Journal of biomedical materials research Part A,* 84(2), 523-534.

Luz, G. M., & Mano, J. F. (2012). Chitosan/bioactive glass nanoparticles composites for biomedical applications. *Biomedical materials,* 7(5), 054104.

Mendonça, G., Mendonça, D. B., Aragao, F. J., & Cooper, L. F. (2008). Advancing dental implant surface technology–from micron-to nanotopography. *Biomaterials,* 29(28), 3822-3835.

Muzzarelli, R. A. (2011). Chitosan composites with inorganics, morphogenetic proteins and stem cells, for bone regeneration. *Carbohydrate Polymers,* 83(4), 1433-1445.

Namvar, N., Salahinejad, E., Saberi, A., Baghjeghaz, M. J., Tayebi, L., & Vashaee, D. (2017). Toward reducing the formation temperature of diopside via wet-chemical synthesis routes using chloride precursors. *Ceramics International,* 43(16), 13781-13785.

Oshida, Y. (2010). *Bioscience and bioengineering of titanium materials*: Elsevier.

Ponsonnet, L., Reybier, K., Jaffrezic, N., Comte, V., Lagneau, C., Lissac, M., & Martelet, C. (2003). Relationship between surface properties (roughness, wettability) of titanium and titanium alloys and cell behaviour. *Materials Science and Engineering: C,* 23(4), 551-560.

Rahmani, H., & Salahinejad, E. (2018). Incorporation of monovalent cations into diopside to improve biomineralization and cytocompatibility. *Ceramics International*.

Ren, K., Dusad, A., Zhang, Y., & Wang, D. (2013). Therapeutic intervention for wear debris-induced aseptic implant loosening. *Acta Pharmaceutica Sinica B,* 3(2), 76-85.

Salahinejad, E., & Baghjeghaz, M. J. (2017). Structure, biomineralization and biodegradation of Ca-Mg oxyfluorosilicates synthesized by inorganic salt coprecipitation. *Ceramics International,* 43(13), 10299-10306.

Salahinejad, E., & Vahedifard, R. (2017). Deposition of nanodiopside coatings on metallic biomaterials to stimulate apatite-forming ability. *Materials & Design,* 123, 120-127.

Shukla, A., & Balasubramaniam, R. (2006). Effect of surface treatment on electrochemical behavior of CP Ti, Ti–6Al–4V and Ti–13Nb–13Zr alloys in simulated human body fluid. *Corrosion Science,* 48(7), 1696-1720.

Singh, R., & Dahotre, N. B. (2007). Corrosion degradation and prevention by surface modification of biometallic materials. *Journal of Materials Science: Materials in Medicine,* 18(5), 725-751.

Takeda, S., Yamamoto, K., Hayasaka, Y., & Matsumoto, K. (1999). Surface OH group governing wettability of commercial glasses. *Journal of non-crystalline solids,* 249(1), 41-46.

Textor, M., Sittig, C., Frauchiger, V., Tosatti, S., & Brunette, D. M. (2001). *Properties and biological significance of natural oxide films on titanium and its alloys*. In *Titanium in medicine* (pp. 171-230): Springer

Vahedifard, R., & Salahinejad, E. (2017). Microscopic and spectroscopic evidences for multiple ion-exchange reactions controlling biomineralization of CaO. MgO. 2SiO2 nanoceramics. *Ceramics International,* 43(11), 8502-8508.

Valerio, P., Pereira, M. M., Goes, A. M., & Leite, M. F. (2004). The effect of ionic products from bioactive glass dissolution on osteoblast proliferation and collagen production. *Biomaterials,* 25(15), 2941-2948.

Yamaguchi, S., Takadama, H., Matsushita, T., Nakamura, T., & Kokubo, T. (2009). Cross-sectional analysis of the surface ceramic layer developed on Ti metal by NaOH-heat treatment and soaking in SBF. *Journal of the Ceramic Society of Japan,* 117(1370), 1126-1130.

Zhao, L., & Chang, J. (2004). Preparation and characterization of macroporous chitosan/wollastonite composite scaffolds for tissue engineering. *Journal of Materials Science: Materials in Medicine,* 15(5), 625-629.